2011

Review of free-space optical communications with diverging beam

Yuchi Zhang
Michigan Technological University

REVIEW OF FREE-SPACE OPTICAL COMMUNICATIONS WITH DIVERGING BEAM

By
Yuchi Zhang

A REPORT
Submitted in partial fulfillment of the requirements for the degree of
MASTER OF SCIENCE

(Electrical Engineering)

MICHIGAN TECHNOLOGICAL UNIVERSITY
2011

This report, “Review of Free-Space Optical Communication with Diverging Beam,” is hereby approved in partial fulfillment of the requirements for the Degree of MASTER OF SCIENCE IN ELECTRICAL ENGINEERING.

Electrical and Computer Engineering

Signatures:

Report Advisor: _____

Zhijun Zhao

Committee Member 1: _____

Zhijun Zhao

Committee Member 2: _____

Warren Perger

Committee Member 3: _____

Yu Cai

Department Chair: _____

Daniel R. Fuhrmann

Date: _____

Abstract

The report reviews the technology of Free-space Optical Communication (FSO) and simulation methods for testing the performance of diverged beam in the technology. In addition to the introduction, the theory of turbulence and its effect over laser is also reviewed. In the simulation revision chapter, on-off keying (OOK) and diverged beam is assumed in the transmitter, and in the receiver, avalanche photodiode (APD) is utilized to convert the photon stream into electron stream. Phase screens are adopted to simulate the effect of turbulence over the phase of the optical beam. Apart from this, the method of data processing is introduced and retrospected. In the summary chapter, there is a general explanation of different beam divergence and their performance.

Contents

List of Figures

List of Tables

Acknowledgement

My greatest appreciation goes to my academic advisor, Dr. Zhijun Zhao, who took me in as his graduate student and offered me the opportunity, advices, guidance and encouragement to finish my master's degree and this report.

Each of my family members deserves special recognition for endless love and encouragement during this endeavor: many sacrifices of time ensured my success.

Chapter 1

Introduction of Free-space Optics

1.1 Technology Overview

In the past decade, Free-space Optical Communication (FSO) has indicated a prospective future in various applications [1]. Due to the character of wireless and straight line communication link with a high transmitting speed, FSO has shown several advantages over other competitors.

1.1.1 Free-space Optical Communication and the "Last Mile" Problem

In optical communication, the "last mile" problem is always a bottleneck restriction over the total speed of the network: as the construction of laying of optical fiber in downtown areas is always expensive and time consuming, most designers will choose to load the signal on exist cables, which slows down the access speed from user into the optical network. A new substitute for optical fiber that has a lower cost and similar transition speed is necessary to promote optical fiber technology.

FSO has a similar speed as optical fiber (Giga bps level), which means it will not slow

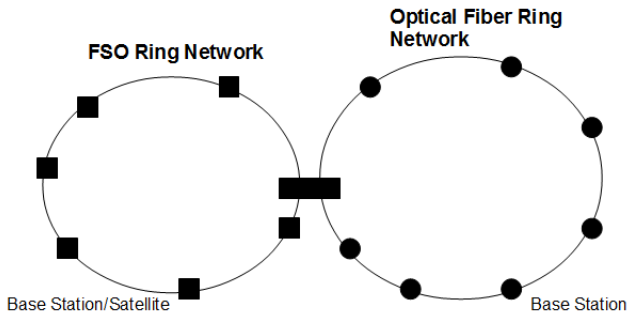

Figure 1.1: An application of FSO in backbone optical network

down the speed of the backbone network. It can be taken as an ideal solution to the "last mile" problem found in commercial applications. Due to its wireless character, FSO is also a more economical way of solving the "last mile" problem. Compared to traditional optical fiber or cable networks, FSO is an efficient choice in construction(no road digging) and data transmitting(similar speed with optical fiber)[1].

Apart from high-speed and wireless, the straight line communication character makes FSO a secure high-speed communication with no license fee. As the signal travels in a straight line, the whole communication channel is in the "visible" area from the transmitter, and any tapping activity will be detected right after its sensor being put between the transceivers. In addition to security, the FSO signals are not likely to interfere each other when they all go in a straight line, which means the band resources of FSO can be used repeatedly as long as those two transmitters do not aim at the same receiver, so compared to the general wireless system, no license is necessary to manage the band resources.

1.1.2 Typical Applications of FSO

The commercial applications of FSO can be viewed either in the network layer aspect or in the physical layer aspect. In the network layer, there are applications in either

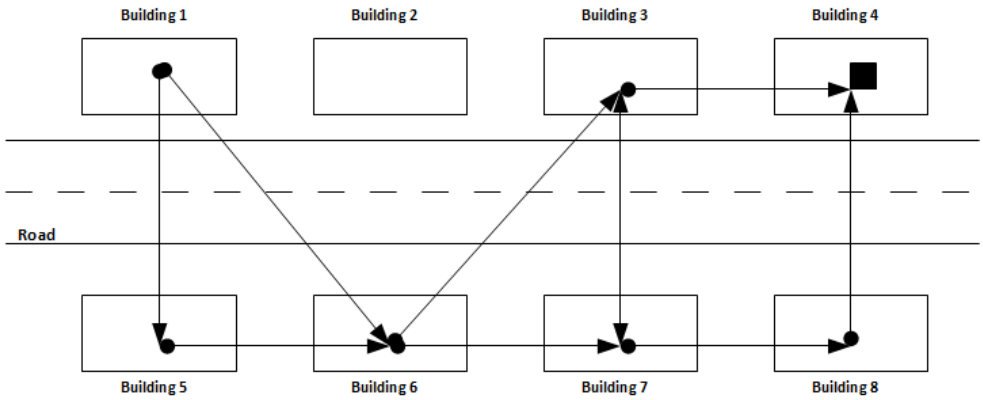

Figure 1.2: An application of FSO network in urban area

the backbone optical network or the easy-establishing building area optical network. In backbone networks, FSO transceivers are linked to switchers, base stations or even satellites, as is shown in Figure 1.1. For the reason that FSO does not slow down the optical fiber communication at some speed levels, the FSO technology can set up an optical network with similar speed and standard but with a lower budget.

Figure 1.2 shows an example of using FSO technology to set up an optical network in an urban area: In an urban area that contains several buildings of certain heights, optical network transceivers are put on top of the buildings seated over the roads[2][3], each building will be taken as a node in the topping map. If the topology is well designed, different route can be found to maintain the connection between any two nodes in the topping map when the original link is down.

In physical layer application, there exists a large range of FSO devices that vary from the transceivers pair that can work behind a glass window to the transceiver that establish the link between a base station on the earth and a satellite on the orbit. Compared to using optical fiber, FSO systems are more practical, and are more faster compared to 802.11 wireless LAN, which can reach only 300Mbps. Apart from this, FSO systems also have a good performance in system robustness, during the New York terrorist attack

when the fiber optic links were destroyed, FSO was used to re-establish a high speed communication link easily and quickly.

1.2 The Channel Characters and Existing Solutions

The channel FSO transmitter facing is the atmosphere. As FSO does not have spectrum problems, the challenge in FSO mainly comes from the signal power. For the matter of signal power in the channel, there are two factors that will have interference over the received signal in the channel: one is the channel noise; another one is channel fading over the signal. For engineering feasibility, the FSO system is required to be non-damaging to humans, which means the power emitted should be strictly controlled under a certain level. In addition to these, there are problems like transmitter jitter, solar effect, network robustness, etc.

The signal emitted has to go through the turbulent atmosphere that causes channel fading. Turbulence can be formed by the unequal distribution of humidity and temperature in different parts of the atmosphere. It can make the irradiance intensity of the optical beam fluctuate randomly, which, in physics, is called scintillation. In sense of communication, the scintillation will cause attenuation and beam wandering at the receiver (even the transmitter does not move) and eventually random fading is observed. It can also be expected that when the propagating distance is increasing, the random fading in channel also increases. Apart from turbulence, some types of gases in atmosphere will also absorb the energy of the laser in the air, which decreases the laser power when the propagating distance increases. The power absorption will also lead to fading in the FSO communication system.

As the laser used for FSO belongs to infrared (IR) in the electro-magnetic spectrum, any source that emits infrared waves around will be a source of background noise to the signal in the receiver. Consider the fact that many kind of thermal radiation emit IR in

a city area, which means the background noise sources are quite usual, and can be taken as a white noise. Besides, the noise is not likely to be correlated with the transmitter signal, the noise can be taken as additional white noise.

The base the FSO transceivers are usually fixed is at the top of a building, which means it also has random movement called jitter. This movement can be caused either by wind, small scale earthquake, or even a slammed door in the building. Such movement may make the laser beam wander at the receiver, which may cause misalignment between two transceivers if it exceeds a certain level. Transceiver jitter can also be found in the inter-satellite FSO link[4] and airplane-satellite link.

There have already been several solutions towards the problems listed above. Beam tracking has already been proven to be effective in solving the beam wandering(either from transmitter jitter or turbulence). And two laser windows(780-850nm, 1520-1600nm, infrared area)[5] were raised where the absorption of the laser power is low. Similar to RF communication, the wavelength filter is also adopted to lower the power of noise over the signal in use. Some kinds of coding[6] have proven effective in making the information in the signal more robust over the channel fading with certain level.

1.3 Previous Work Summary

To settle the challenges described in section 1.2, several research groups did different work to explore the communication models. In experimental methods, approaches like numerical simulation and physical experiment were performed to explore the turbulence and its effect on the communication link[7][8][9][10]. Several solutions like coding[6], beam focusing[11] and beam diverging[4][12][13] were raised for communication link enhancement or other specific applications, which has a common goal of increasing the Signal to Noise Ratio(SNR) and decreasing Bit Error Rate (BER) of the receiving signal.

Previously, there has already been some researches focusing on the aspect of communication. Kiasaleh[7] derived a probability of fading in the FSO channel based on the assumption of the Log-normal distributed normalized irradiance (Log-normal Distribution, LN). The Log-normal distributed normalized irradiance (Log-normal Distribution, LN) is described by Fried[14] to be a model derived based on several assumptions under ideal conditions, and following simulations[15] and experiments have made it clear that the log-normal cannot perfectly describe the condition of the corresponding data. Al-Habash and Andrews [16]pointed out that the log-normal distribution underestimates the peak and the tail performance of measured data, and derived a model of gamma-gamma distribution. The gamma-gamma function has a good agreement in both weak and strong turbulence as well as a good convergence property, but latter researches[15] also figured out the problems in the function that will limit is further application in commercial design.

In addition to theoretical derivation, researches using simulation methods and experiment methods also exists. Zhao and his team[17][18][6][19][13] used the simulation method to discover the performance of FSO system with different coding modulation algorithms and tracking equipment. They directly use the data of power distribution from the simulation to avoid the weakness from different power distribution models, and made several valuable conclusions in the sense of communication. Stromqvist, Young, Andrews and Recolons performed an experiment in Australia in 2007[15] to compare the data from experiment, simulation and existing models. The result also showed that the model of log-normal and gamma-gamma still do not show good agreement with the simulation and experiment data when considering its tail in both strong and weak turbulence.

In the application of the diverge technology, there are works focusing on solving the problem of relative moves within a communication link. Toyoshima [4] explored using diverge technology to improve inter-satellite optical communication by solving the satellite jitter effect by enlarging the transmitter beam's diverging angle. LoPresti[12] did

his research on using diverged beam to carry the signal to control a moving vehicle. In the opposite direction of diverge technology, Recolons and Andrews [11] explained the effect of focusing the laser beam and reached a conclusion that the tracking system has a better performance if applied on a system with focused beam rather than the general collimated beam.

1.4 The Free-Space Optical Communication System and Structure

1.4.1 FSO in Communication System

The model of modern communication system is shown in Figure 1.3. FSO is the communication whose physical layer uses laser in general atmosphere to carry the modulated signals. The optical transmitter of an FSO communication system can be compared to a transmitter antenna in general wireless communication; and its optical receiver part can be compared to a receiving antenna in general wireless communication.

The research of FSO actually concerns the input of the formal step and the output of latter step of the FSO within the whole system: the transmitted signal can only be compared to the received signal in a readable format, such that the BER is taken to judge the reliability of the system. In addition, the distribution of optical signal power at the receiving aperture helps to measure the fading performance of the channel and eventually it will still interference the system BER. The signal goes into the laser sensor can be taken as a combination of channel effect over the signal, the noise from channel, and alignment mistake caused by transmitter jitter.

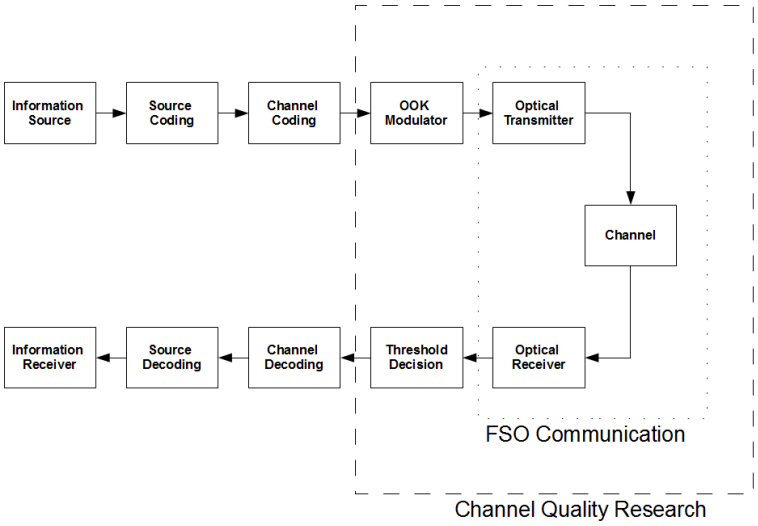

Figure 1.3: The position of free-space optical communication system in digital communication

1.4.2 System Composition

In a general FSO model like Figure 1.4, the system is generally made of several components: the laser emitter generates the On-Off-Keyed (OOK) modulated optical signal; the transmitter lens make the optical wave into a previously designed form: collimated, diverge or focused; the receiver aperture collects the optical signal that has fading from turbulent channel with additive white noise (AWN), and inject them into the optical sensor, which is taken as Avalanche Photodiode (APD) in this report, where the optical signal should be converted into an OOK modulated electrical signal if in an ideal condition.

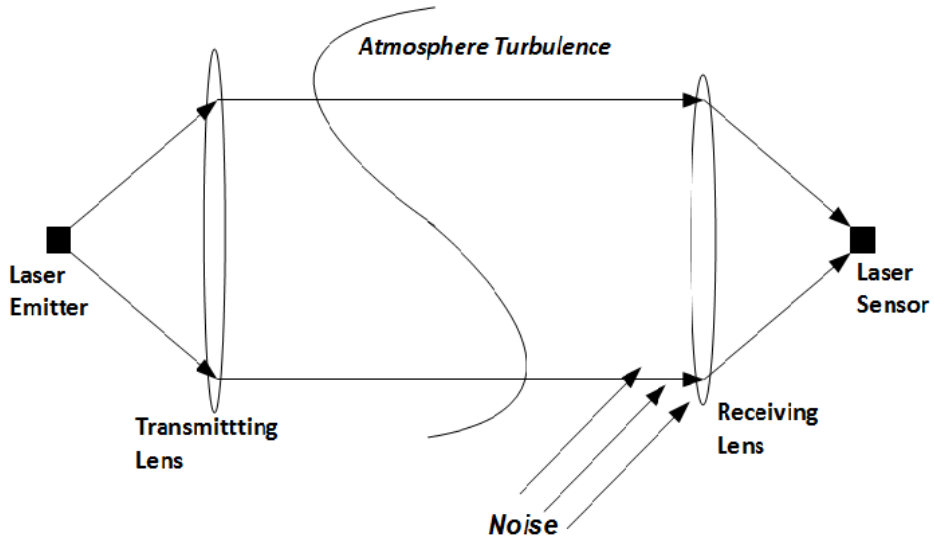

Figure 1.4: The model of a collimated free-space optical communication system

1.4.3 Signal Description

As in the system described, the OOK modulated signal right coming from the transmitter with time parameter t can be modeled as $s_t(t)$, then the signal at the receiver will be:

$$s_r(t) = s_t(t)h(t) + s_n(t) \tag{1.1}$$

Where the fading parameter, $h(t)$ refers to the channel effect over the signal at different time, which may be a composition of attenuation, spectrum broadening, beam waive changing, beam wandering etc., and $s_n(t)$ refers to the background noise which can be modeled by additional white noise.

The distribution of the power of the received signal ($s_r(t)$) is studied to describe the specification of channel fading, and the goal of studying channel fading is to increase the SNR and thus decrease BER for general purpose communication link.

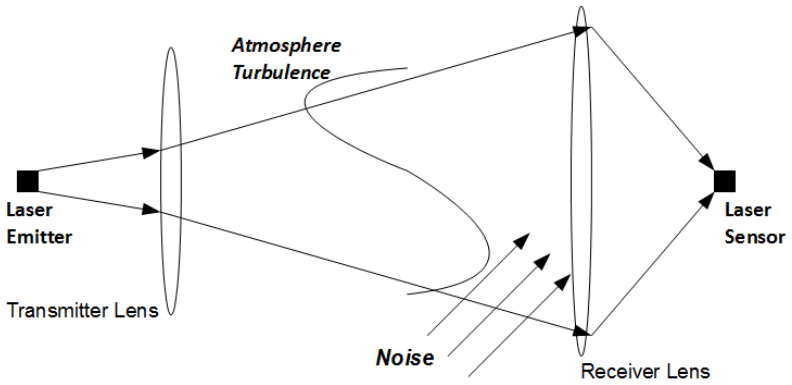

Figure 1.5: The model of a diverged free-space optical communication system

1.4.4 Beam Focus and Diverge in FSO

As is shown in Figure 1.5, the focal distance of the transmitter lens is adjusted to diverge the laser beam in the FSO system as compared to Figure 1.4. Such a way is adopted to enlarge the beam spot at the receiver, and it is expected that using this way can enhance the performance of the link. Previous works[18] showed that the best receiving effect happens when a specific receiving aperture diameter meets the specific distance, while the distance can change the spot size and irradiation intensity (fading factor $h(t)$ in equation (1.1)) as the turbulence level is related with propagating distance, and both of which can also be interfered by changing the diverging angle of the beam at the transmitter.

1.5 Report Composition

The rest of the report describes the FSO Communication with focused/diverged beam in a more detailed way. Chapter 2 describes the laser scintillation in the atmosphere including the turbulence theory and the effect of turbulence over the irradiance intensity,

and Chapter 3 introduces the method of realization of the scene discussed in Chapter 2 in the numerical simulation and the way of taking laser irradiance into consideration. Finally in Chapter 4 there is a general summary of the report and a summary of the analysis.

Chapter 2

Basic Turbulence Theory and Laser Power Fluctuation

2.1 Komolgorov Turbulence Theory

2.1.1 The Reynold Number and Turbulence Strength Measurement

According to the view of Andrews[20], Kolmogorov turbulence is considered to be caused by the turbulent flow. The turbulent flow forms a velocity field, and its intensity is measured by the Reynold Number given by[20].

$$R_e = \frac{V \cdot \mathbf{l}}{v} \tag{2.1}$$

In equation (2.1), V is the characteristic velocity magnitude of the velocity field, $\mathbf{l}$ is the direction of flow, and v is defined to be the kinematic velocity (m^2/s). From the definition equation(Equation (2.1)), the Reynold number grows according to the strength of turbulence, and if the Reynold number is in the order of 10^5, the Kolmogorov turbulence

is considered to be high.

2.1.2 Kolmogorov's Assumption

Based on the definition of Reynold Numbers, Kolmogorov made the following two assumptions:

(1) Reynold numbers are considered to be sufficiently large, which means small-scale structure turbulence is statistically homogeneous, isotropic, and independent of large-scale structure. The definition of small-scale and large-scale turbulence will be explained in section 2.1.3.

(2) The motion with small-scale turbulence is uniquely determined by the kinematic velocity (recorded as v) and average rate of dissipation(recorded as ϵ) with the unit (m^2/s^3).

2.1.3 Turbulence Process

As is shown in previous sections, in the case of velocity turbulence, the Kolmogorov turbulence is caused by a velocity field[20]. When the character velocity increases, the Reynold Number increases according to its definition given by equation (2.1). When the Reynold Number exceeds a critical value, there generates unstable local air masses are generated, called "eddies." By the assumptions in section 2.1.2, the eddies are independent of parent flow in character direction ($\mathbf{l}$ in equation (2.1)).

As there are inner forces in eddies, the original generated eddies reduce and becomes into small eddies, in contrast, the original eddies are called "large eddies." In this process, the inner scale l_0 and outer scale L_0 is defined for eddies with measure l': If $l_0 < l' < L_0$, the eddies are in the inertial subrange; if $l' < l_0$, the eddies are in the viscous dissipation

range and if $l' > L_0$, the eddies are not independent of parent flow.

In general, the inner scale is between 1 mm and 10 mm in near ground atmosphere, while it can be in centimeters in the troposphere and stratosphere.

When eddies are getting smaller, their energy is dissipated, and as a result, the dissipated energy matches the kinetic energy of parent flow. In this condition, the Reynold number is about 1, and the correlated eddy scale is l_0.

2.1.4 Structure Function of Turbulent Spaces

Kolmogorov showed longitudinal structure function of a velocity field with a direction parallel to the vector that connects two observation points $D_{RR}(\mathbf{R})$[20].

$$D_{RR}(\mathbf{R}) =< (\mathbf{V}_1 - \mathbf{V}_2)^2 >= C_V^2 \cdot |\mathbf{R}|^{\frac{2}{3}} \tag{2.2}$$

Here, there is $l_0 \ll |\mathbf{R}| \ll L_0$ and vector $\mathbf{R}$ connects two points $\mathbf{V}_1$ and $\mathbf{V}_2$, and C_V is the velocity structure constant with $C_V = 2\epsilon^{\frac{2}{3}}$. ϵ is the average energy dissipation rate.

As to the range of $|\mathbf{R}|$, the inner scale l_0 is comparable to the Kolmogorov microscale: $\eta_K = (v^3/\epsilon)^{\frac{1}{4}}$, while the outer scale is $L_0 \sim \epsilon^{\frac{1}{2}}$, where ϵ refers to the dissipation rate, and the stronger the dissipation is, there is stronger turbulence with smaller inner scale and larger outer scale.

In addition, when $|\mathbf{R}| \ll l_0$ (i.e. in deep viscous dissipation area), the structure function will be $D_{RR}(\mathbf{R}) = C_V^2 l_0^{-\frac{4}{3}} |\mathbf{R}|^2$. the structure function of the inertial subrange in three dimensional condition is $\Phi_{RR} = 0.066\epsilon^{\frac{2}{3}}\kappa^{-\frac{11}{3}} = 0.033 C_V^2 \kappa^{-\frac{11}{3}}$ where κ is the scalar special frequency with a domain $\frac{1}{L_0} \ll \kappa \ll \frac{1}{l_0}$.

2.1.5 Turbulence Conditions in Other Cases

Apart from velocity turbulence, there is also other turbulence caused by other facts. One reason that causes turbulence is temperature, temperature fluctuation is a passive and does not exchange energy with the velocity turbulence[20]. And there are longitudinal temprature fluctuations which is given by[20]:

$$D_T(|\mathbf{R}|) =< (T_1 - T_2)^2 >= \begin{cases} C_T^2 l_0^{-\frac{4}{3}} |\mathbf{R}|^2 & 0 \leq |\mathbf{R}| \ll l_0 \\ C_T^2 |\mathbf{R}|^{\frac{2}{3}} & l_0 \ll |\mathbf{R}| \ll L_0 \end{cases} \tag{2.3}$$

where T_1 and T_2 means the temperature at two observation points over a position difference of $\mathbf{R}$ and C_T^2 is the temperature structure constant. Here the inner scale l_0 is defined with diffusivity in the air D and dissipation rate ϵ by[20]:

$$l_0 = 5.8(D^3/\epsilon)^{1/4} \tag{2.4}$$

In a three dimensional conditions, the fluctuation spectrum of turbulence caused by temperature difference will be[20]:

$$\Phi_T(\kappa) = 0.033 C_T^2 \kappa^{-\frac{11}{3}} \tag{2.5}$$

where the spacial frequency (magnitude) κ meets the inertial subrange requirement: $\frac{1}{L_0} \ll \kappa \ll \frac{1}{l_0}$. The definition of Kolmogorov power spectrum will be shown in Section 2.1.6.

Andrews[20] described a fluctuation caused by the changing of reflective index. Ishimaru[21] had a similar description over a condition that the reflective particles are randomly distributed in the medium and the medium scatters the laser propagated through.

Given a specified position $\mathbf{R}_1$ with a time parameter t, there is random reflective index $n(R,t)$[20]:

$$n(\mathbf{R}_1,t) = n_0 + n_1(\mathbf{R}_1,t) \tag{2.6}$$

where n_0 is the average reflective index, with the assumption that the random medium discussed here is atmosphere, $n_0 = 1$. Therefore, the parameter of reflective index fluctuation n_1 has to be zero mean, so that the overall reflective index has a unit mean. In the atmosphere, the Equation (2.6) will be[20]:

$$n(\mathbf{R}_1,t) = 1 + n_1(\mathbf{R}_1,t) \tag{2.7}$$

If it is further restricted into the case that only optical waves and infrared waves are propagated in the medium. The overall reflective index will be approximated as[20]:

$$n(\mathbf{R}_1) \approx 1 + 79 \times 10^{-6} \cdot \frac{P(\mathbf{R}_1)}{T(\mathbf{R}_1)} \tag{2.8}$$

where $P(\mathbf{R}_1)$ denotes the pressure at $\mathbf{R}_1$ in millibars, $T(\mathbf{R}_1)$ refers the temperature at $\mathbf{R}_1$ in kelvin.

The spatial structure function in this condition is[20]:

$$D_n(\mathbf{R}) = \begin{cases} C_n^2 l_0^{-\frac{4}{3}} |\mathbf{R}|^2 & 0 \leq |\mathbf{R}| \ll l_0 \\ C_n^2 |\mathbf{R}|^{\frac{2}{3}} & l_0 \ll |\mathbf{R}| \ll L_0 \end{cases} \tag{2.9}$$

In Equation (2.9), C_n^2 to be the index of refraction structure constant. $l_0 = 7.4\eta = 7.4(\frac{v^3}{\epsilon})^{\frac{1}{4}}$, and in experiment, scintillometer can be used to measure the path averaged

value of C_n^2 and l_0.

2.1.6 Kolmogorov Power Spectrum

Given a random value field, there is covariance of two points denoted by $\mathbf{R}_1$ and $\mathbf{R}_2$ by definition[20]:

$$B_n(\mathbf{R}_1, \mathbf{R}_2) \equiv B_n(\mathbf{R}_1, \mathbf{R}_1 + \mathbf{R}) =< n_1(\mathbf{R}_1) n_1(\mathbf{R}_1 + \mathbf{R}) > \tag{2.10}$$

where $|\mathbf{R}| = |\mathbf{R}_1 - \mathbf{R}_2|^2$, if $\mathbf{R}_1$ is set to be zero in the coordinates, the covariance can be written as $B_n(\mathbf{R})$. With the property of Fourier Transformation, there is power spectrum of reflective index fluctuation(Here $\mathbf{R}$ is taken to be in the 3 scalars in the 3D integrity)[20]:

$$\Phi_n(\mathbf{k}_f) = \frac{1}{(2\pi)^3} \int B_n(\mathbf{R}) e^{-i \cdot \mathbf{k}_f \cdot \mathbf{R}} d\mathbf{R} \tag{2.11}$$

and the inverse Fourier Transform:

$$B_n(\mathbf{R}) = \frac{4\pi}{\mathbf{R}} \int_0^\infty \mathbf{k}_f \Phi_n(\mathbf{k}_f)(1 - \frac{\sin \mathbf{k}_f \mathbf{R}}{\mathbf{k}_f \mathbf{R}}) d\mathbf{k}_f \tag{2.12}$$

where, the $|\mathbf{k}_f| = \kappa$ and $\mathbf{k}_f$ is the position index in frequency space. In the Free-space Optics model, temperature fluctuation causes the reflective index fluctuation. The power spectrum of temperature fluctuation is generally adopted for the power spectrum of reflective index fluctuations[20].

$$\Phi_n(\kappa) = 0.033 C_n^2 \cdot \kappa^{-\frac{11}{3}} \tag{2.13}$$

Here, the spatial frequency (scalar) κ fulfills the condition $\frac{1}{L_0} \ll \kappa \ll \frac{1}{l_0}$, in the application, the inner scale and outer scale take extreme values: $L_0 = \infty$ and $l_0 = 0$.

2.2 Laser Propagation in Turbulent Media

Ishimaru[21] has described a general map of the methods to analyze the problem of electro-magnetic wave's propagation in the atmosphere, the "transport theory" and the "analytical theory". The problem discussed here is based on the theory with the analytical method.

2.2.1 Laser Propagation in Random Medium

From Maxwell's formula, the requirements that the optical wave must meet during the propagation in the turbulent medium with random reflective index can be derived[20].

$$\nabla^2\mathbf{E} + k^2n^2(\mathbf{R}_1)\mathbf{E} + 2\nabla[\mathbf{E}\cdot\nabla log(n\mathbf{R}_1)] = 0 \tag{2.14}$$

Here, $\mathbf{E}$ is the vector amplitude of propagating the electromagnetic wave; $k = \frac{2\pi}{\lambda}$ is the wave number; $n(\mathbf{R}_1)$ is the refractive index at position $\mathbf{R}_1$, and ∇ is the Laplace operator i. e. $\frac{\partial^2}{\partial x^2} + \frac{\partial^2}{\partial y^2} + \frac{\partial^2}{\partial z^2}$.

As the turbulence is caused by the random refractive index, in order to keep the Maxwell equations (Equation (2.14)) remains constant, the vector amplitude of the electromagnetic wave has to be a random number based on some distribution which correlates with the fading factor ($h(t)$ in Equation (1.1)) directly.

In order to simplify the problem, there are some assumptions taken to get the approximations of the problem according to the statement by Andrews[20]. One of the assumptions

is the time discrete assumption: time variations in the refractive index are sufficiently slow, which means the time is constant for a single condition.

Apart from the time variance, there are the following assumptions:

(1) The backscattering of the wave can be neglected.

(2) The depolarization effects can be neglected.

(3) The refractive index is delta correlated in the direction of propagation.

(4) The parabolic (paraxial) approximation can be invoked.

Based on these assumptions, the problem can be expressed to find an amplitude that meets the following Maxwell Equations[20]:

$$\nabla^2 \mathbf{E} + k^2 n^2(\mathbf{R}_1) \cdot \mathbf{E} = 0 \tag{2.15}$$

It can also be further simplified if the wave vector $\mathbf{E}$ was changed into a scalar value U if the dimension is fixed. If turbulence is limited in the refractive index turbulence, by assumption (3), it can be derived to be[20]:

$$n(\mathbf{R}_1) = n_0(\mathbf{R}_1) + n_1(\mathbf{R}_1) \tag{2.16}$$

where $n_0(\mathbf{R}_1) = n_0 =< n(\mathbf{R}_1) >= 1$ and $< n_1(\mathbf{R}_1) >= 0$. There also exists the correlation function of refractive index[20]:

$$< n(\mathbf{R}_1)n(\mathbf{R}_2) >=< n_1(\mathbf{R}_1)n_1(\mathbf{R}_2) >= B_n(\mathbf{R}_1 - \mathbf{R}_2) \cong \delta(z_1 - z_2)A_n(\mathbf{r}_1 - \mathbf{r}_2) \tag{2.17}$$

Using Wiener-Khinchin theorem, there is the Fourier transform with correlation and power spectrum[20].

$$B_n(\mathbf{R}_1, \mathbf{R}_2) = B_n(\mathbf{R}_1 - \mathbf{R}_2) = \int_{-\infty}^{+\infty} \Phi_n(\mathbf{k}_f) \cdot e^{i \cdot \mathbf{k}_f \cdot \mathbf{R}} d\mathbf{k}_f \equiv \delta(z) A_n(\mathbf{R}) \tag{2.18}$$

where $\mathbf{R} = \mathbf{R}_1 - \mathbf{R}_2$ and $z = z_1 - z_2$, such that[20]:

$$A_n(\mathbf{R}) = 2\pi \int \int_{-\infty}^{+\infty} \Phi_n(\mathbf{k}_{f2}) e^{i \cdot \mathbf{k}_{f2} \cdot \mathbf{R}} dk_x dk_y \tag{2.19}$$

As in Equation (2.19) $\delta(z) = 1$ is assumed (ie, $k_z \equiv 0$), the frequency vector is taken to be $\mathbf{k}_{f2} = (k_x, k_y)$ (compared to Equation (2.18), where $\mathbf{k}_f = (k_x, k_y, k_z)$)

In some works like Andrews[22], Zhu[9] etc, the turbulence is assumed to be isotropic. In these conditions, the Fourier transform will be in a more simplified form according to Andrews[20]:

$$A_n(R) = 4\pi^2 \cdot \int_0^{+\infty} k \cdot \Phi_n(k) J_0(kR) dk \tag{2.20}$$

where, $R = |\mathbf{R}|$ and $J_0(x)$ is the zero-order Bessel function of the first kind.

2.2.2 Rytov Variance and the Measure of Turbulence Intensity

The Rytov Variance is used to measure the turbulence intensity in FSO communication models, and it is defined as[21]:

$$\sigma_R^2 = 1.23 C_n^2 k^{\frac{7}{6}} L^{\frac{11}{6}} \tag{2.21}$$

where C_n^2 is the refractive index structure parameter, $k = \frac{2\pi}{\lambda}$ is the wave number of the electromagnetic wave, and L is the path length the electromagnetic wave passes through.

In case that $\sigma_R^2 < 1$, the laser is thought to be in weak fluctuations. When $\sigma_R^2 \sim 1$, the turbulence causes moderate fluctuations, the electromagnetic wave experiences strong turbulence and turbulence of the saturation regime if $\sigma_R^2 > 1$ and $\sigma_R^2 \to \infty$ respectively.

In the case of the Gaussian wave, weak fluctuation is labeled with the following two conditions that are both fulfilled[21]:

$$\sigma_R^2 < 1 \text{ and } \sigma_R^2 \Lambda^{\frac{5}{6}} < 1 \tag{2.22}$$

where $\Lambda = \frac{2L}{kW^2}$ and W is the free space beam radius at the receiver. There is another function taken to label the weak fluctuation with the plane wave condition[21]:

$$q < 1 \text{ and } q \cdot \Lambda < 1 \tag{2.23}$$

in which $q = \frac{L}{k \cdot \rho_{pl}^2}$ and ρ_{pl}^2 is the coherent radius of the plane wave.

2.2.3 Rytov's Approximation of the Analytical Representation

Up to now, there is no solution to Equation (2.14). Even its simplified forms only have approximation solutions. Andrews[20] showed Born's approximation in his book, and both Andrews[20] and Ishimaru[21] introduced Rytov's approximation, which has directional meaning in turbulence simulation.

The Rytov's approximation assumes the solution is in the form of the complex phase[21]:

$$u(\mathbf{R}_1, t) = u_0(\mathbf{R}_1, t)e^{\psi(\mathbf{R}_1, t)} \tag{2.24}$$

where, $\psi(\mathbf{R}_1, t)$ is the complex phase of the electro-magnetic wave, and $u_0(\mathbf{R}_1, t)$ is the field with definite amplitude and phase (i.e. a no turbulence field is taken as a reference). In general $u_0(\mathbf{R}_1, t) =< u(\mathbf{R}_1, t) >$. As the wave is a complex phase, it can be simplified that[21]

$$\psi(\mathbf{R}_1, t) = \chi(\mathbf{R}_1, t) + iS_1(\mathbf{R}_1, t) \tag{2.25}$$

If the electro-magnetic wave ,u and u_0, are expressed in amplitude (A and A_0), and phase, (S and S_0) respectively, which means[21]

$$\begin{cases} \chi(\mathbf{R}_1, t) = ln(\frac{A}{A_0}) \\ S_1(\mathbf{R}_1, t) = S(\mathbf{R}_1, t) - S_0(\mathbf{R}_1, t) \end{cases} \tag{2.26}$$

which means $\chi(\mathbf{R}_1, t)$ is the amplitude fluctuation in the logarithm form called "log-amplitude" fluctuation, and $S_1(\mathbf{R}_1, t)$ is the fluctuation of phase(generally, the average phase is zero).

In the case of line-of-sight, the electro-magnetic wave experiences amplitude and phase fluctuation in some thin layers in cascade. The field can be written as[21]:

$$u = u_0 \cdot \prod_{i=1}^{n} u_i \tag{2.27}$$

where i represents the number of layers and there is exponential representation of the

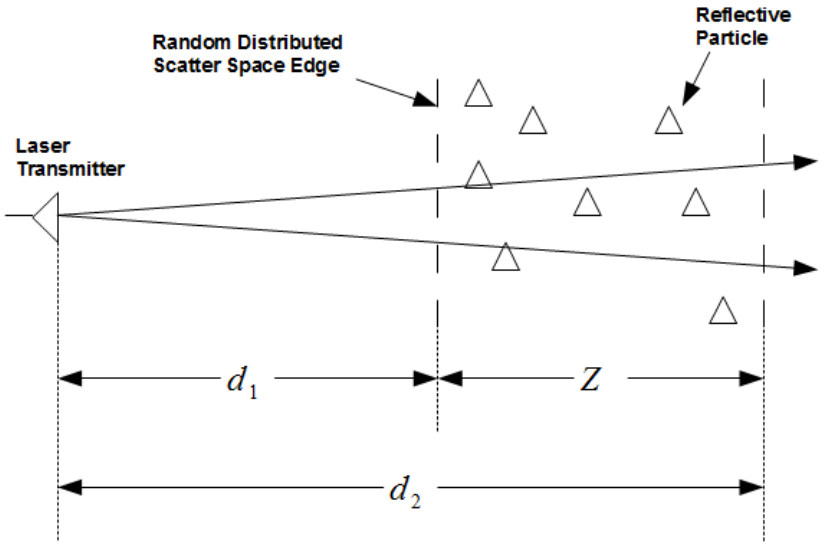

Figure 2.1: The condition when laser is transmitted to a space with randomly distributed reflective scatters

field[21]:

$$u = u_0 \cdot e^{\sum_{i=1}^{n} \psi_i} \tag{2.28}$$

From the complex phase, there is Rytov's approximation solution[21]:

$$\psi(\mathbf{R}_1) = \int_V \frac{\mathbf{f}(\theta)}{d_1} e^{(ik - \frac{\rho\sigma_t}{2}) \cdot d_1 (1 - cos\theta)} \tag{2.29}$$

where ρ is the density of the scattering disk in a specific space, $\mathbf{f}(\theta)$ is the scattering amplitude, which is also a complex number, that "represents the amplitude, phase and polarization of the scattered wave in the far field in the direction $\mathbf{o}$"[21], and the parameter θ in Reference [21] is illustrated as in Figure 2.2 from Reference [21]. d_1 is the distance between the close edge of the turbulence space and the laser emitter as is illustrated in Figure 2.1 from Reference [21] (In phase screen simulation, it is the distance of closer border of the phase screen to the transmitter lens). In the case of FSO, there

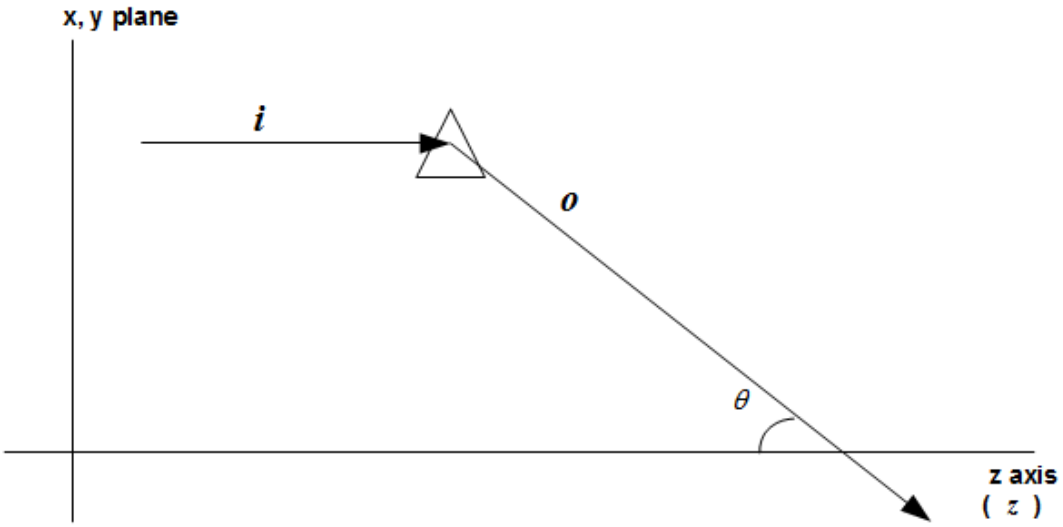

Figure 2.2: The condition when laser is hit on to a single reflective particle

is a relation between reflective particle size(D) and system scale: $D \ll (\lambda L)^{1/2}$, where L is the propagating distance of the system scale and λ is the wavelength of the carrier laser; then there is an atmosphere correlational function[21]:

$$\begin{cases} B_\chi(d) = \frac{\rho\sigma_s L}{2} \cdot \frac{sin(kd)}{kd} & \text{if } D < \lambda \\ B_\chi(d) = \frac{\rho\sigma_s L}{2} \cdot e^{-\frac{(kd)^2}{4\alpha_P}} & \text{if } D > \lambda \end{cases} \tag{2.30}$$

in Equation (2.30), $d = |\mathbf{R}_1 - \mathbf{R}_2|$, ρ is the density of the scattering disk in the space, σ_s is the scattering cross section, which has[21]

$$\sigma_s = \int_{4\pi} \sigma_d dw = \int_{4\pi} |\mathbf{f}(\mathbf{o}, \mathbf{i})|^2 dw \tag{2.31}$$

where $\alpha_P = 2.77/\theta_b^2$ where θ_b is the half power beam width (in radians) of the particle scattering pattern.

In the case when $D \ll (\lambda L)^{1/2}$, the variance of amplitude fluctuation is[21]

$$< \chi^2 >= \frac{\rho \cdot \sigma_s \cdot L}{2} \tag{2.32}$$

From Equation (2.32), there is irradiance intensity (power of electro-magnetic wave in turbulence)[21]:

$$I = | < u > |^2 \cdot < e^{2\chi} >= e^{-\rho\sigma_t L} \cdot < e^{2\chi} > \tag{2.33}$$

Assume that the log-amplitude χ is normally distributed, which means[21]

$$< e^{2\chi} >= e^{2<\chi>+2<(x-<x>)^2>} \tag{2.34}$$

with the previous assumption $< \psi >=< \chi > +i < S_1 >= 0$, and replace the $< e^{2\chi} >$ in Equation (2.33) with Equation (2.34), such that[21]

$$I = e^{-\rho \cdot \sigma_t \cdot L} \cdot < e^{2\chi^2} >= e^{-\rho \cdot \sigma_a \cdot L} \tag{2.35}$$

There are several remarks in Equation (2.35) and Equation (2.33): σ_t is the total cross section[21]:

$$\sigma_t = \sigma_s + \sigma_a \tag{2.36}$$

where σ_a is the absorption cross section; the amplitude square average in this section is assumed to have attenuation effect only such that[21]

$$I_t =< I >=< |u|^2 >= e^{-\rho\sigma_a z} \tag{2.37}$$

Chapter 3

System Structure and Simulation Methodology

3.1 System Structure and Signal Simulation

3.1.1 System Structure

In simulation, the total system can be divided into 3 parts based on the paper[13]:

1. Transmitter: this part includes the transmitting power, transmitting signal modulating and beam diverging in the transmitter.

2. Channel Simulation: This part includes the power attenuation, turbulence simulation, receiving power distribution and SNR (Signal-Noise Ratio) calculation at the receiver.

3. Receiver Model: The simulation adopts APD receiver with McIntyre-Conradi model, and BER (Bit Error Rate) is calculated at the output of the receiver.

3.1.2 Signal Model

Considering that the McIntyre-Conradi model[23][24] is based on the input of photon numbers, the overall signal is converted into photon numbers compared to the signal model in Equation (1.1)[19].

$$n_r(t) = n_t(t)h(t) + n_b(t) \tag{3.1}$$

where $n_b(t)$ is the background noise photon number, $n_t(t)$ is the transmitted photon number at the transmitter's aperture, $n_r(t)$ is the number of received photons at the receiver's aperture, and $h(t)$ is still the channel fading over the transmitted photon.

The number of received photons meet Poisson distribution, which means[18]

$$n_t(t) \sim \text{Poisson}(\mu_t) \tag{3.2}$$

$$n_b(t) \sim \text{Poisson}(\mu_b) \tag{3.3}$$

$$n_r(t) \sim \text{Poisson}(\mu_r) = \text{Poisson}(\mu_t(t)h(t) + \mu_b(t)) \tag{3.4}$$

And the probability distribution function (PDF) of Poisson distribution is given by[19]

$$P_P(v;\mu) = \frac{\mu^v e^{-\mu}}{v!} \tag{3.5}$$

where, μ refers to the expectation of the random number, $v = 1, 2, 3 \ldots$ is the number of

Table 3.1: The parameters for space model used by Zhao

Pixel Size	5 mm × 5 mm
Phase Screen Resolution	512 × 512
Phase Screen Size	2.5 m × 2.5 m
Number of Phase Screen	10

events that happen in a given time period. The mean photon number μ_t is believed to be the linear combination of the mean photon numbers for both "on" and "off" conditions. The received mean photon number μ_r is believed to be the result of channel effect over average transmitted photon numbers, which means[21]

$$\mu_r = \mu_t \cdot h(t) + \mu_b \tag{3.6}$$

$$\mu_t = p_{on} \cdot \mu_{on} + (1 - p_{on}) \cdot \mu_{off} \tag{3.7}$$

3.1.3 Space Model

In the simulation, total space is discretized into several phase screens. Each phase screen is also discretized into pixels. Take Zhao's paper[19] as an example, each pixel has a size of 5 mm × 5 mm, there are 512 × 512 pixels in each phase screen, and each phase screen has a size of about 2.5 m × 2.5m. Table 3.1.3 is the conclusion of the discretized space in Zhao's paper[19].

For each simulation, the spatial structure parameter is fixed and the correlational coefficient between two points are fixed.

3.2 Signal Transmission

3.2.1 Signal Modulation

The signal is on-off keyed (OOK) before it is finally sent into the atmosphere. According to the definition[25], in the optical OOK modulation: symbol 1 is represented by emitting an optical pulse of constant amplitude with a certain duration and symbol 0 is represented by emitting optical pulse of another different amplitude with same duration. According to the definition, the average photon number for each 1 and 0 condition has the following relation:

$$\mu_T(t) = \begin{cases} \mu_{T0} & \text{if } x(t) = 0 \\ \mu_{T1} & \text{if } x(t) = 1 \end{cases} \tag{3.8}$$

where $x(t)$ represents the sequence of the base band signal. Assuming $h_0(t)$ is the attenuation factor between the laser source and the transmitting aperture, the relationship between $\mu_t(t)$ and $\mu_T(t)$ is[19]:

$$\mu_t(t) = h_0(t)\mu_T(t) \tag{3.9}$$

3.2.2 Beam Divergence

At the transmitter, the beam diverging (or focusing) lens is applied to diverge (or to fucus) the beam from the transmitting lens. In the simulation, this effect is represented by the focal distance of beam diverging (or focusing) lens l_f, and different l_f are taken to view the effect of divergence towards the optical signal receiver.

3.3 Channel Simulation

As is described by Lane[26], the optical beam is affected by its phase distortion more than other facts. The phase screen technology is adopted to simulate the effect of turbulence that causes beam wandering. One phase screen is an atmosphere of certain thickness that lies in the path the laser propagates through, and its area is large enough to cover the beam waist to affect the optical beam by its turbulence.

3.3.1 Phase Screen Simulation

The core idea of phase screen simulation is the two dimensional Fourier transformation pair to obtain phase fluctuation spectrum ($P_h(\mathbf{k})$) from phase fluctuations ($p_f(\mathbf{r})$):

$$P_h(\mathbf{K}) = \int_{-\infty}^{+\infty} p_f(\mathbf{r}) e^{-i2\pi(\mathbf{r}\cdot\mathbf{K})} d\mathbf{r} \tag{3.10}$$

and

$$p_f(\mathbf{r}) = \int_{-\infty}^{+\infty} P_h(\mathbf{K}) e^{-i2\pi(\mathbf{K}\cdot\mathbf{r})} d\mathbf{K} \tag{3.11}$$

where $\mathbf{r} = (x, y)$ is the position vector of the points in the phase fluctuation (frequency domain), $\mathbf{K}$ is the position vector in the phase fluctuation spectrum in the spatial domain when the thickness of the phase screen is considered.

As is shown in Figure 3.3.1, the total propagation path of the laser beam is divided into several phase screens in cascade. In each phase screen, the Fourier transform is used to convert between laser amplitude and laser phase.

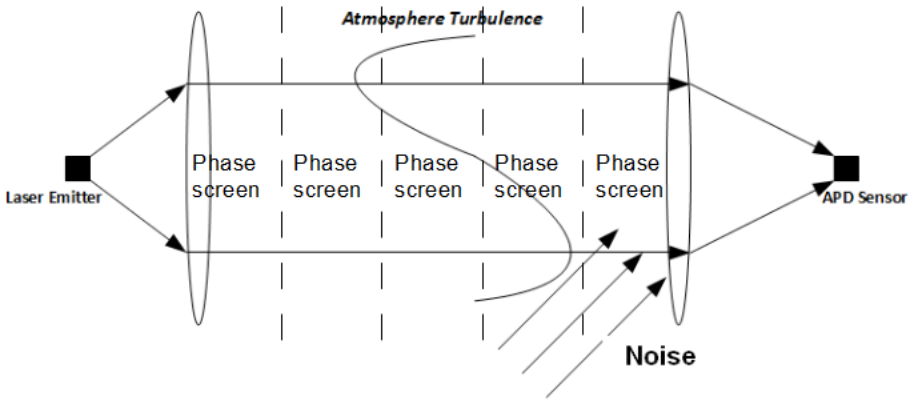

Figure 3.1: The schematic diagram of phase screen in FSO

3.3.2 Realization of Phase Screen Simulation

There are several algorithms that can realize the purpose of simulating the fluctuation in phase of a laser beam in the air. Vetelino[15] described a simulation method in his paper and pointed it out that the method meets the experiment result they did in 2005. The method they adopted is as follows.

In their algorithm, they first randomly generate a normally distributed spectrum screen (frequency domain) with zero mean and variance to be $< |A_{\mu\nu}|^2 >$, where $A_{\mu\nu}$ is the harmonic wave amplitude that meets[15]:

$$< |A_{\mu\nu}|^2 >= 2\pi \cdot k^2 \cdot \Delta z \cdot \Phi_n(\mathbf{K}_{\mu\nu}) \cdot (\Delta s_g)^2 \tag{3.12}$$

where k is the propagating field wave number, Δz is the thickness of the phase screen, Δs_g is the grid spacing in the phase screen and $\Phi_n(\mathbf{K}_{\mu\nu})$ is the spectral power density (power spectrum) at the position represented by vector $\mathbf{K}_{\mu\nu}$. Here, Kolmogorov's power spectrum with reflecting index fluctuation (Equation (2.13)) is adopted in discretized form to represent the power density.

By two dimensional Fourier transform (showed in Equation (3.10) and Equation (3.11)), the power spectrum screen is converted into the phase fluctuation screen (2-D spatial domain), the phase of the wave is obtained. By the structure of cascade of the phase screens, the phase of the laser signal is passed on, and finally, the phase at the receiver can be estimated by summing the interferences together.

3.3.3 Improvements for Phase Screen Generation

Apart from the simulation algorithm mentioned in Section 3.3.2, several algorithms have been raised to improve the performance of phase screen simulations. The algorithms can be divided into two categories: One is for the case when the amplitude distribution can not be accurately obtained but spatial correlation of the two points in the space is achievable; another one is that in order to either improve the accuracy of the simulation or accelerate the simulation, interpolation technology is adopted to estimate some points in the phase screen.

The algorithm that uses covariance matrix is described by Goldring[27] but not used[28]. In the paper, each phase screen is assumed to have P points and there are Q layers of screen in the propagation path, and Cholesky decomposition is used to divide the covariance matrix into two matrixes that each one is the transpose of another[28].

$$\Gamma_h = \mathbf{P}_h \mathbf{P}_h^T \tag{3.13}$$

Then a random value vector $\mathbf{A}$ is generated according to[28]:

$$\mathbf{A} = [a_i] \sim N(0, 1) \tag{3.14}$$

where the index $i = 1, 2, 3 \cdots P \times Q$, The residue phase in the pupil grid (ie, the output

of the set of phase screen) can be drawn as[28]:

$$\phi = \mathbf{P}_h \mathbf{A} \tag{3.15}$$

Here, the vector $\mathbf{A}$ is transformed into a matrix sequence that have the same size with $\mathbf{R}$. The algorithm can be verified by[28]:

$$< \phi\phi^T >=< \mathbf{P}_h\mathbf{A}(\mathbf{P}_h\mathbf{A})^T >=< \mathbf{P}_h\mathbf{A}\mathbf{A}^T\mathbf{P}_h^T >= \mathbf{P}_h < \mathbf{A}\mathbf{A}^T > \mathbf{P}_h^T = \mathbf{P}_h\mathbf{P}_h^T = \Gamma_h \tag{3.16}$$

The interpolation algorithm is also described by several researchers[29][30]. The aim of these algorithms can be concluded as using 2-D interpolation to improve the simulation accuracy by increasing the screen resolution, and to increase the simulation speed by using interpolation to represent some of the sampling points without sacrificing the resolution of the phase screen.

3.4 Receiver Model

3.4.1 The Receiver Structure

The receiver has a structure shown in Figure 1.5. At the receiver's aperture, the turbulence is averaged over the aperture and the photons are collected by a receiving lens. When the received beam is being injected into the Avalanche Photodiode (APD) from receiving aperture, the optical beam suffers the fluctuation from the atmosphere between the APD and the aperture. As the receiver's structure is similar to the laser emitter's, the turbulence caused by such fluctuation can be recorded as[19]:

$$\mu_i(t) = h_0(t)\mu_r(t) \tag{3.17}$$

where $\mu_i(t)$ represents the average photon number that will be sent into the photon detector; $h_0(t)$ is the fading parameter in the channel, with the similar structure, the fading factor can be taken as same as the one in the transmitter; $\mu_r(t)$ is the average number of photons that is collected by the aperture.

3.4.2 Avalanche Photodiode Detector

The avalanche photodiode detector is adopted in this simulation as a photon-electrical converter in the receiver. With a comparatively high efficiency in optical-electrical conversion, APD is also widely used as an optical detector not only in optical communications of different forms but also in other optical detection areas. There are many models developed to describe the performance of APD in optical detection. The McIntyre-Conradi model[23][24] is one of those that accurately plots the performance of APD, and the Webb model [31] describes the simplified models that are easy for simulation calculating and are accurate in large input conditions. In the FSO communication, the receiver lens is not likely to collect an input that is "large" enough. Accurate McIntyre-Conradi model is adopted for APD performance, although it is more computationally complicated.

In the McIntyre-Conradi model, the APD performance is described as a conditional probability of photon number (input) and electron number (output). If given the photon number n and the number of electron m, there is conditional probability[19][24]:

$$P_T(m|n) = \begin{cases} \frac{n\times\Gamma(\alpha_m+1)}{m(m-n)!\Gamma(k_I\alpha_m+1+n)} \times [\frac{1+k_I(\bar{G}-1)}{\bar{G}}]^{n+k_I\alpha_m} \times [\frac{(1-k_I)(\bar{G}-1)}{\bar{G}}]^{m-n} & m \geq n \\ 0 \qquad m < n \\ 1 \qquad m = n = 0 \end{cases} \tag{3.18}$$

Γ refers to the gamma function, $\bar{G}$ is the average gain of the APD, k_I is the ionization ratio and there is replacement: $\alpha_m = \frac{m}{1-k_I}$.

By Equation (3.18), and considering that the number of photons that goes into the receiving aperture obeys the Poisson distribution, which is given by[19]

$$P(y(t)) = \sum_{n_i=0}^{y(t)} P_T(y(t)|n_i(t))P_P(n_i;\mu_i(t)) \tag{3.19}$$

Here, $y(t)$ represents the number of electrons in the output electric pulse sequence from APD detector, and the dark current and the therm noise of APD is omitted from the equation as their effects are taken to be far less than the background noise. n_i and μ_i is the input photon number and the average input photon number correspondingly, P_P is the Poisson distribution defined in Equation (3.5), and P_T is the transportation probability of APD defined in Equation (3.18). Considering the channel effect from the receiving aperture to the APD receiver, and substituting the $\mu_n(t)$ with Equation (3.17) and the received signal model Equation (3.1), there is presentation of the electron number in a certain pulse[19]:

$$P(y(t)) = \sum_{n_i=0}^{y(t)} P_T(y(t)|n_i(t))P_P(n_i;h_0h(t)\mu_t(t)+\mu_b) \tag{3.20}$$

3.5 Data Processing Strategy

With the simulation method, it can be expected that the signal before APD is a random number sequence with some distribution, and the distribution will affect the final bit error rate (BER) after it is converted into electron flows with APD. The data processing strategy can be divided into two main aspects: the receiving power distribution and bit error rate (BER) analysis.

3.5.1 Receiving Power Distribution

In the receiving power distribution, the first job is to quantify the distribution, either with a function if there is close form solution or a series that can model the trend of the distribution function.

Up to now, the closed form solution of the distribution function is not available, so in practise, when the received signal from simulation is at 10^5 level, the calculation complexity will be too much if using the whole histogram to estimate the series when too many randomness will be included in the function. A possible solution of compromising is to adjust the histogram bin that makes the data size of the histogram is both large enough for accurate description and small enough to keep good processing speed.

The procedure for analyzing the receiving quality can be concluded as follows:

(1) Make the histogram of the received data and normalize the histogram to make it in a scale of distribution.

(2) Adjust the histogram bin that will make it good enough for the computer to find a series to describe the distribution.

3.5.2 Communication Quality Analysis

The communication quality of this FSO link is determined by BER. The electrical signal amplitude distribution can be obtained by the transition function as in Equation (3.20) if the optical intensity distribution is known. As the transmitting modulation is OOK, which is also known, the received bit error rate is then achievable.

Chapter 4

Summary

The report introduces the technology of Free Space Optical communication and the problem that the technology is facing. Based on the problem, the theory of turbulence is discussed with its effect over laser beam, and there concludes Kolmogorov spectrum with Equation (2.13):

$$\Phi_n(\kappa) = 0.033 C_n^2 \cdot \kappa^{-\frac{11}{3}} \tag{4.1}$$

Apart from that, the review of the Rytov solution displayed a general figure of the laser in the turbulent atmosphere. The simulation and data processing method is also introduced to illustrate the general methodology for simulation.

Figure 4.1 is a schematic diagram of a cross-section in the receiving plane in the simulation space. Due to the fact that a photon stream is shot toward the center of receiving aperture, the power distribution of the optical signal is expected to be similar to the red dash curve displayed in Figure 4.1, where the horizontal axis represents the position at the receiving plane in the space, and the blue curve represents the additive white noise which is assumed to have a uniformly distributed value on the whole receiving plane. In

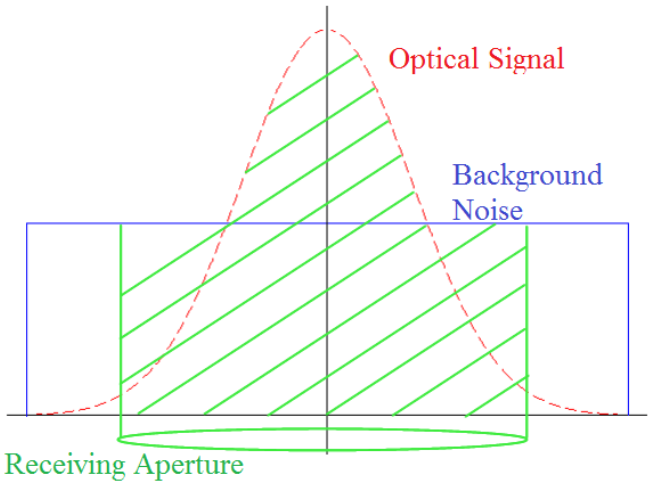

Figure 4.1: The optical signal at receiving(schematic diagram)

Figure 4.1, the vertical axis is the center of the receiving plane, which is also assumed to be the target of the transmitted laser beam. The green lens at the bottom is the size of a receiving lens, and the shadowed green part is the energy collected by the aperture.

From Figure 4.1, it can be figured out that the receiving aperture is actually collecting the same noise power through out its aperture, but the SNR has a trend of going down if the receiving aperture is getting large. Therefore it can be expected that the optimum moment in receiving occurs when the receiving aperture collects the signal and noise at a portion (the receiving aperture do not necessarily collect all the signal) that maximizes the signal to noise ratio(SNR). This explains why for different propagating distances, it is the receiving aperture of some specific size that makes the optimum receiving effect, rather than "the bigger the better." There is similar reason for the diverged beam, while the diverged beam has a "fatter" and "shorter" red dash curve as shown in Figure 4.2, it will also change the receiving aperture size for optimum receiving. For the tracked system that uses focused beam, the signal curve will be "taller" and "thinner", when there are "steeper" increasing and decreasing edges as is shown in Figure 4.3, which means when the center moves, the receiving aperture will lead to a larger SNR changing than the collimated beam or diverged beam. Based on the "steeper" signal curve, when

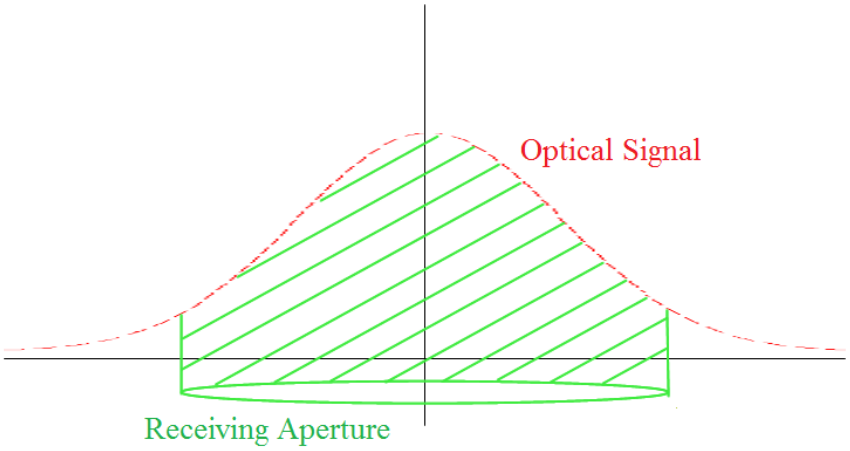

Figure 4.2: The schematic diagram of diverged optical signal at receiving plane

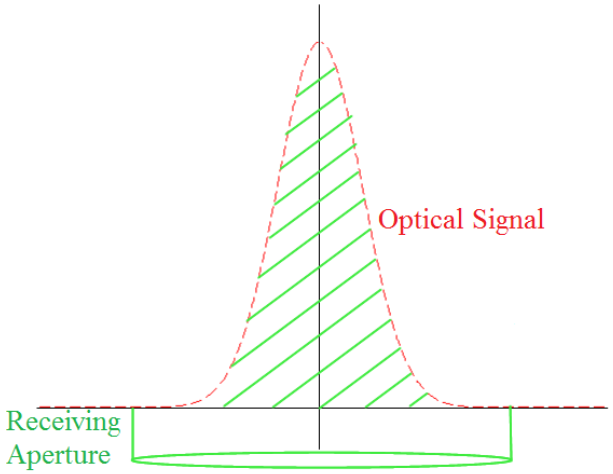

Figure 4.3: The schematic diagram of focused optical signal at receiving plane

a tracking system is added to an FSO link, which can eliminate the beam wandering to a large extent[17], more signal power will be stably collected in the aperture, and thus the system with tracking system and focused beam has a better performance than the one uses collimated beam and same tracking system.

Bibliography

[1] D. Killinger, "Free-space optics for laser communication through the air," *Optics & Photonics News*, vol. 13, no. 10, pp. 36–42, 2002.

[2] D. Kedar and S. Arnon, "Urban optical wireless communication networks: the main challenges and possible solutions," *Communications Magazine, IEEE*, vol. 42, no. 5, pp. s2–s7, 2004.

[3] H. A. Willebrand and B. S. Ghuman, "Fiber optics without fiber," *Spectrum, IEEE*, vol. 38, no. 8, pp. 40–45, 2001.

[4] M. Toyoshima, T. Jono, K. Nakagawa, and A. Yamamoto, "Optimum divergence angle of a Gaussian beam wave in the presence of random jitter in free-space laser communication systems," *J. Opt. Soc. Am. A*, vol. 19, no. 3, pp. 567–571, 2002.

[5] S. Bloom, E. Korevaar, J. Schuster, and H. Willebrand, "Understanding the performance of free-space optics[invited]," *Journal of optical networking*, vol. 2, no. 6, pp. 178–200, 2003.

[6] Z. Zhao, R. Liao, S. D. Lyke, and M. C. Roggermann, "Reed-Solomon coding for free-space optical communications through turbulent atmosphere," in *Proceedings of IEEE Aerospace Conference*, (Big Sky, MT), pp. 1–12, March 2010.

[7] K. Kiasaleh, "Performance analysis of free-space, on-off-keying optical communication system impaired by turbulence," in *Proc. of SPIE*, vol. 4635, (Free-Space Laser Communication Technologies XIV, San Jose, CA, USA), pp. 150–161, January 2002.

[8] J. A. Anguita, M. A. Neifeld, and B. V. Vasic, "Spatial correlation and irradiance statistics in a multiple-beam terrestrial free-space optical communication link," *Applied Optics*, vol. 46, no. 26, pp. 6561–6571, 2007.

[9] X. Zhu and J. N. Kahn, "Free-space optical communication through atmospheric turbulence channels," *IEEE Transactions on Communication*, vol. 50, no. 8, pp. 1293–1300, 2002.

[10] J. C. Ricklin and F. M. Davidson, "Point-to-point wireless communication using partially coherent optical fields," in *Proceedings of SPIE*, vol. 4489, (Free-Space Laser Communication and Laser Imaging, San Diego, CA, USA), pp. 156–165, July 2002.

[11] J. Recolons, L. C. Andrews, and R. L. Phillips, "Analysis of beam wander effects for a horizonal-path propagating Gaussian-beam wave: focused beam case," *Opt. Eng.*, vol. 46-086002, pp. 1–11, 2007.

[12] P. Lopresti, H. Refai, J. Sluss, and I. Valera-Cuadrado, "Adaptive divergence and power for improving connectivity in free-space optical mobile networks," *Applied Optics*, vol. 45, no. 25, pp. 6591–6597, 2006.

[13] Z. Zhao, R. Liao, and Y. Zhang, "Impacts of laser beam diverging angle on free-space optical communications," in *Proceedings of IEEE Aerospace Conference*, (Big Sky, MT), pp. 1–10, March 2011.

[14] D. L. Fried, "Statistics of laser beam fade induced by pointing jitter," *Applied Optics*, vol. 12, pp. 422–423, 1973.

[15] F. Stromqvist Vetelino, C. Young, L. Andrews, and J. Recolons, "Aperture averaging effects on the probability density of irradiance fluctuations in moderate-to-strong turbulence," *Applied Optics*, vol. 46, pp. 2099–2108, 2007.

[16] M. Al-Habash and L. Andrews, "Mathmatical model for the irradiance probability density function of a laser beam propagating through turbulent media," *Opt. Eng.*, vol. 40, pp. 1554–1562, 2001.

[17] Z. Zhao, S. D. Lyke, and M. C. Roggermann, "Adaptive optical communication through turbulent atmospheric channels," in *Proceedings of ICC '08. IEEE International Conference on Communications*, (Beijing), pp. 5432–5436, May 2008.

[18] Z. Zhao, R. Liao, S. D. Lyke, and M. C. Roggermann, "Direct detection free-space optical communications through atmospheric turbulence," in *Proceedings of IEEE Aerospace Conference*, (Big Sky, MT), pp. 1–9, March 2010.

[19] Z. Zhao and R. Liao, "Effects of beam wander on free-space optical communications through turbulent atmosphere," in *Proc. of SPIE 7685*, (Atmospheric Propagation VII, Orlando, Florida, USA), pp. K1–K12, April 2010.

[20] L. C. Andrews and R. L. Phillips, *Laser Beam Propagation Through Random Media*. SPIE - The International Society of Optical Engineer, P.O. Box 10 Bellingham, WA, 98227-0010, USA: SPIE Press, 2006.

[21] A. Ishimaru, "Theory and application of wave propagation and scattering in random media," *Proceedings of IEEE*, vol. 65, no. 7, pp. 1030–1061, 1977.

[22] L. Andrews, R. Phillips, and P. Yu, "Optical scintillations and fade statistics for a satellite-communication system," *Applied Optics*, vol. 34, pp. 7742–7751, 1995.

[23] R. J. McIntyre, "The distribution of gains in uniformly multiplying avalanche photodiodes: theory," *IEEE Transactions on Electron Devices*, vol. Ed-19, pp. 703–713, 1972.

[24] J. Conradi, "The distribution of gains in uniformly multiplying avalanche photodiodes: experimental," *IEEE Transaction on Electron Devices*, vol. Ed-19, pp. 713–718, 1972.

[25] S. Haykin and M. Moher, *Introduction to Analog & Digital Communiations (Second Edition)*. John Wiley & Sons, 111 River St. Hoboken, NJ, 07030-5774, USA: Wiley, 2007.

[26] R. G. Lane, A. Glindemann, and J. C. Dainty, "Simulation of a Kolmogorov phase screen," in *Waves in Random Media*, pp. 209–224, 1992.

[27] T. Goldring and L. Carlson, "Anaysis and implementation of non-Kolmogorov phase screens appropriate to structured environments," in *Nonlinear optical beam manipulation and high energy beam propagation through the atmosphere, Proceedings of the Meeting*, pp. 244–264, January 1989.

[28] M. C. Roggemann, B. M. Welsh, D. Montera, and T. A. Rhoadarmer, "Mehtod for simulating atmoshpheric turbulence phase effects for multiple times slices and anisoplanatic conditions," *Applied Optics*, vol. 34, pp. 4137–4051, 1995.

[29] C. M. Harding, R. A. Johnston, and R. G. Lane, "Fast simulation of a Kolmogorov phase screen," *Applied Optics*, vol. 38, pp. 2161–2170, 1999.

[30] J. Recolons and F. Dios, "Accurate calculation of phase screens for the modelling of laser beam propagation through atmospheric turbulence," *Porc. of SPIE*, vol. 589107, pp. 1–12, 2005.

[31] P. P. Webb, M. R. J., and J. Conradi, "Properties of avalanche photodiodes," *RCA Review*, vol. 35, pp. 234–278, 1974.